Cement and Concrete Research 138 (2020) 106251

Contents lists available at ScienceDirect

Cement and Concrete Research

journal homepage: www.elsevier.com/locate/cemconres

Calcium sulfoaluminate clinker hydration at different alkali concentrations

P. Padilla-Encinas, A. Palomo, M.T. Blanco-Varela, A. Fernández-Jiménez*

Eduardo Torroja Institute for Construction Science (IETcc-CSIC), Madrid, Spain

ARTICLE INFO

Keywords:
Calcium sulfoaluminate clinker
NaOH concentration
^{27}Al MAS-NMR

ABSTRACT

This paper discusses the effect of alkalis on strength development and hydration products in a commercial calcium sulfoaluminate clinker (KCSA). KCSA pastes were hydrated with water and 0.1 M, 1 M, 2 M, 4 M and 8 M NaOH. The hydration products were characterised at 3d, 28d and 90d, by XRD, SEM, DTA/TG and ^{27}Al MAS-NMR. With 0.1 M, 1 M and 2 M, the main hydration products were similar to those observed in the water-hydrated pastes: ettringite, AH_3 and calcium aluminate hydrates such as CAH_{10}; ^{27}Al MAS-NMR analysis revealed different degrees of crystallinity in AH_3. With 4 M and 8 M, ettringite was not detected, AH_3 crystallinity rose and siliceous hydrogarnet, calcium carboaluminate hydrates, thenardite and calcite were formed at higher alkalinity. Sample carbonation, which grew more intense with time and at higher alkalinity, yielded calcium carbonate and an aluminium hydroxide gel inducing cracking.

1. Introduction

Inasmuch as calcium sulfoaluminate cement (CSA) requires a firing temperature ~200 °C lower than portland cement (PC), its production is less energy-intensive [1]. It also releases less CO_2 both for that reason and due to the lower limestone content in the raw mix. Those eco-benefits have prompted recent research interest in CSA cements [2–7]. Such cements are normally blended, primarily with PC, to produce high early age strength and rapid setting and hardening binders able to offset drying shrinkage [4,5].

CSA cements comprise calcium sulfate and CSA clinker (KCSA), whose mineralogy consists primarily in ye'elimite, belite, calcium aluminates and calcium sulfates. Ye'elimite ($4CaO.3Al_2O_3.SO_3$), also known as Klein's compound, is the majority phase, accounting for around 50% of the total. When ye'elimite is hydrated with water the reaction products are calcium monosulfoaluminate hydrate (AFm) and microcrystalline aluminium hydroxide (AH_3) (Eq. (1)) [8]. If hydrated with excess water, small amounts of ettringite and C_3AH_6 may also form (Eq. (2)). Although these hydrates co-exist, ettringite (AFt) ultimately converts to AFm [3]. That development may be associated with the capacity of AFm to form a solid solution with OH-AFm (C_4AH_{13}) [9], in which some of the sulfate ions are replaced by hydroxide. As a result, some sulfate would be available to form ettringite as per Eq. (2). Other authors [10,11], however, contend that the reaction involved may be as described in Eq. (3), with ettringite, katoite and (monosulfide-free) aluminium hydroxide forming in the absence of sulfates.

$$C_4A_3\,\bar{S} + 18H \rightarrow C_4A\bar{S}H_{12} + 2AH_{3\,(microcystalline)} \quad (1)$$

$$4\,C_4A_3\,\bar{S} + 80H \rightarrow C_6A\bar{S}_3H_{32} + C_4A\bar{S}H_{12} + 2C_3AH_6 + 8AH_3 \quad (2)$$

$$3\,C_4A_3\bar{S} + 62H \rightarrow C_6A\bar{S}_3H_{32} + 2\,C_3AH_6 + 6\,AH_3 \quad (3)$$

Winnefeld et al. studied [8] CSA cement hydration in the $Ca_4Al_6O_{12}SO_4$-Ca_2SiO_4-$CaSO_4$-H_2O system. Their thermodynamic model predicted the possible formation of metastable phases such as CAH_{10} in the presence of a low anhydrite/ye'elimite ratio in the first 1 d to 3 d and their decomposition after 28 d. This hydrate may form as an intermediate product of the hydration of calcium aluminates present in CSA clinker or directly via ye'elimite hydration, which also yields ettringite and an amorphous aluminium hydroxide, as per Eq. (4) [12].

$$3\,C_4A_3\,\bar{S} + 98H \rightarrow C_6A\bar{S}_3H_{32} + 6CAH_{10} + 2AH_{3\,(amorphous)} \quad (4)$$

Any number of studies can be found in the literature on the effect of the type and content of calcium sulfate (anhydrite, bassanite, gypsum) on ye'elimite hydration [13]. The presence of calcium sulfate hastens ye'elimite hydration, giving rise to AH_3 and ettringite needles as in Eq. (5), which induce rapid setting [14].

$$C_4A_3\,\bar{S} + 2C + 38H \rightarrow C_6A\bar{S}_3H_{32} + 2\,AH_3 \quad (5)$$

The hydration of other phases present in CSA clinker such as belite may favour the formation of secondary products. Belite hydration, in turn, yields C-S-H gel and portlandite as per Eq. (6), a slow process [15,16]. However, belite content in CSA clinker or cements is normally low (< 30%) and given the large quantities of AH_3 (from ye'elimite

* Corresponding author.
E-mail address: anafj@ietcc.csic.es (A. Fernández-Jiménez).

https://doi.org/10.1016/j.cemconres.2020.106251
Received 2 April 2020; Received in revised form 30 September 2020; Accepted 30 September 2020
Available online 09 October 2020
0008-8846/ © 2020 Elsevier Ltd. All rights reserved.

Table 1
Chemical and mineralogical analysis of KCSA clinker.

Chemical composition	Mineralogical composition	ICDD[b] no.
CaO = 40.82%	Ye'elimite = 68.4 ± 0.99%	$C_4A_3\overline{S}$ = 33–0256
SiO_2 = 9.51%	Bredigite = 7.40 ± 0.37%	$Ba_{0.293}Ca_{13.467}Mg_{1.81}Mn_{0.43}O_{32}Si_8$ = 36–399
Al_2O_3 = 29.37%	Belite = 16.90 ± 1.03%	C_2S = 86–0398
Fe_2O_3 = 1.32%	Periclase = 3.67 ± 0.21%	MgO = 4–829
MgO = 4.13%	Gehlenite = 1.90 ± 0.44%	$Al_2Ca_2O_7Si$ = 35–755
Na_2O = 1.06%	C_3A = 1.75 ± 0.39%	C_3A = 38–1429
K_2O = 0.47%		
TiO_2 = 0.39%		
SO_3 = 9.92%		
Other = 1.70%		
LoI[a] = 1.31%		

[a] Loss on ignition.
[b] International Centre for Diffraction Data.

hydrations) the reaction described in Eq. (7) prevails [15,17,18], with silicon and calcium reacting with $Al(OH)_3$ to form strätlingite.

$$C_2S + 2H \rightarrow CH + C-S-H \quad (6)$$

$$C_2S + AH_3 + 5H \rightarrow C_2ASH_8 \quad (7)$$

Only blends with at least 35 wt% belite contain sufficient calcium oxide for C-S-H to form as per Eq. (6). Nonetheless, in some cases aluminium absorption by C-S-H gel [19,20] may widen the stability range to include slightly lower belite contents. Strätlingite, which destabilises in the presence of calcium, can react with portlandite to yield siliceous hydrogarnet (Eq. (8)) [21]. Where belite content is > 60%, strätlingite may react with that phase to stabilise C-S-H and katoite as per Eq. (9). Whilst alkalis are known to modify C_2S hydration kinetics in pure phases or PC [16], the effect of their presence on CSA clinkers or cements is poorly understood.

$$CH + C_2ASH_8 \rightarrow C_3ASH_4 \quad (8)$$

$$C_2S + C_2ASH_8 \rightarrow C-S-H + C_3AH_6 \quad (9)$$

Many papers dealing generally with CSA cement and ye'elimite hydration have been published in recent years [22–24], whilst others have addressed the effect of limestone [15,17,21], supplementary cementitious materials (SCMs) such as fly ash [22,25] and organic additions [23,26] on CSA cement hydration. Many gaps in the understanding of the effect of alkalis on CSA cement hydration have yet to be filled, however, despite the research conducted on the subject [22,23,25,26]. According to those studies, alkalis may affect not only the rate of ye'elimite and CSA hydration, but also the nature of the hydration products. The effect of alkalis on CSA and KCSA hydration is an area worth exploring with a view to using these materials as alkaline or alkaline hybrid cement components.

Ogawa et al. [25] observed the presence of 0.05 M to 0.2 M NaOH to hasten ye'elimite hydration. Sánchez et al. [22] found that when ye'elimite was hydrated in 8 M NaOH its initial mechanical strength declined over time due to its conversion to hydrogarnet, thenardite and nordstrandite.

The effect of alkalis on CSA cement (clinker + gypsum) hydration was studied by Zhang et al. [23], who hydrated calcium sulfoaluminate cement with NaOH at concentrations of 0 M, 0.01 M, 0.1 M, 1 M, 5 M and 8 M to examine the microstructural changes taking place in the aluminium hydroxide formed. They observed the degree of AH_3 crystallinity to vary with pH. At low alkalinity, AH_3 crystals were nanoscale and at high concentrations macro-scale, denoting greater crystallinity. In 2019 Durlo Tambara et al. [26] studied commercial CSA cement hydration in 0 M, 0.1 M, 1 M, 4 M and 8 M solutions of NaOH, reporting that at 0.1 M and 1 M the hydration products formed were similar to the ones observed for the reference (water): ettringite and microcrystalline aluminium hydroxide. At the two higher concentrations ettringite was unstable and U-phase and thenardite formed. As these experiments were conducted in the presence of gypsum, however, inducing very rapid initial reactions, the products were difficult to identify with conduction calorimetry. Moreover, the presence of gypsum in the medium affected not only the rate of hydration, but also the nature of the products obtained.

This study aimed to determine the effect of alkalis on commercial CSA clinker (KCSA) hydration in the absence of added sulfates, a system closely resembling the $C_4A_3\overline{S}$ + C_2S + H_2O system. In the experimental design the 4 M and 8 M solutions used to attain the alkalinity required to activate hybrid alkaline cement hydration [27] were supplemented with 0.1 M and 1 M alkaline solutions. The aim was to simulate the high pH prevailing in ordinary portland cement, with which CSA cements are often blended [4,5]. A 2 M solution was studied as an intermediate stage to establish a ceiling value above which medium alkalinity would adversely affect KCSA hydration products.The effect of alkali content on 3 d, 28 d and 90 d mechanical strength development was studied, along with the nature of the hydration products. The hydration products were characterised with XRD SEM, DTA/TG and ^{27}Al MAS-NMR. ^{1}H−^{27}Al cross-polarisation (CP) MAS-NMR was also deployed to differentiate between anhydrous and hydrated aluminate phases and enhance the intensity of the signals of phases with a greater number of OH groups.

2. Experimental procedure

2.1. Materials

The i.tech ALI PRE GREEN industrial calcium sulfoaluminate clinker (KCSA) used in this study was supplied by HeidelbergCement Hispania. Its X-ray fluorescence-determined chemical and X-ray diffraction-determined mineral composition and Rietveld quantification (found with Topas software) are given in Table 1.

As shown by the KCSA clinker particle size distribution in Fig. 1, found on a Coulter LS 130 laser diffractometer with a measuring range of 0.1 μm and 900.0 μm, 90% of the particles were under 35 μm. Clinker density was 2.83 g/mL and its Blaine fineness 408 m^2/kg.

2.2. Procedure

KCSA was hydrated with distilled water and NaOH at concentrations of 0.1 M, 1 M, 2 M, 4 M and 8 M. A constant liquid/KCSA ratio of 0.5 was used to prepare to the pastes. After hand-mixing liquid and clinker for 3 min, mini-slump tests were run to measure paste fluidity in a cone with a 20 mm smaller and 37.5 mm larger diameter. The cone was tapped 10 times as the paste was released to facilitate spread, determined as the mean of measurements taken at four points. The rest of the paste was poured into six 1x1x6 cm moulds to half-height that were then placed on a flow table and tamped 60 times to ensure uniform distribution in the mould and eliminate pores. The moulds were subsequently filled to the top, again tamped 60 times and stored in a

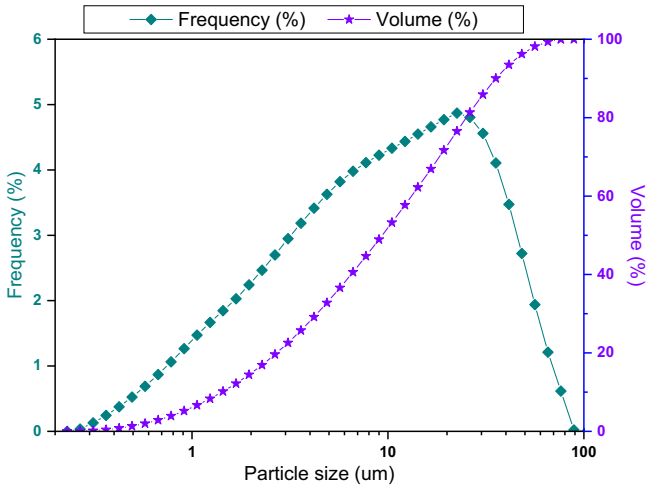

Fig. 1. KCSA particle size.

climate chamber at 21 °C and 95% relative humidity for 24 h. After removal from the moulds the specimens were labelled and stored in the climate chamber for 3 d, 28 d or 90 d, when they were compression tested to failure on an Ibertest Autotest-200/10-SW frame. Strength was established as the mean of the values recorded for six specimens per age.

Part of the material from the broken specimens was ground in an agate mortar and dissolved in isopropanol to detain hydration. The suspension was shaken for 3 min, vacuum-filtered and -dried in a desiccator for 3 d to eliminate the isopropanol. These samples were then characterised with XRD, DTA/TG and NMR. Other (unground) fragments of the broken specimens were soaked in isopropanol for 7 d for use in the scanning electron microscopic (SEM) studies.

XRD analysis was conducted on a Bruker D8 Advance diffractometer with a high-voltage 3 kW generator and a copper anode X-ray tube (Cu K $\alpha_{1,2}$ 1.540 Å radiation), typically operating at 40 kV and 50 mA and coupled to a Lynxeye detector with a 3-mm anti-scatter slit and a (0.5%) Ni K-beta filter, with no monochromator (Kα_2 not eliminated). The settings for qualitative analysis were: variable 6-mm divergence slit at a 2θ angle of 5° to 60°; step time, 0.5 s; step size, 0.02°.

The samples were placed on a platinum crucible in a nitrogen atmosphere for differential thermal and thermogravimetric (DTA/TG) analysis, conducted on a TA SDT Q 600 calorimeter where the temperature was ramped from ambient to 1000 °C at 10 °C/min. Measuring precision was 0.001 °C in DTA and 0.1 μg in TG.

The SEM studies were conducted on a Hitachi 4800 scanning electron microscope with a field emission gun (FEG) and a resolution of 1.4 nm, fitted with a backscattering electron detector (BSEM), a Bruker RX detector, Quantax 400 software for microanalyses and five monitored axes. The vacuum-dried samples were carbon-coated prior to analysis.

The ^{27}Al MAS NMR spectra were acquired at 9.4 T on a Bruker Avance-400 NMR spectrometer at a ^{27}Al resonance frequency of 104.3 MHz, using a spinning frequency of 10 kHz, a 5 s relaxation time, a 2 ms excitation pulse corresponding to a flip angle < 30°, and 400 acquisitions per spectrum. The internal standard for chemical shift measurements (in ppm) was $Al(H_2O)_6^{3+}$. The cross-polarisation (CP) MAS NMR experiments were conducted under the same conditions for ^{27}Al and a 1 ms ^{1}H—^{27}Al contact time. In cross-polarisation magnetisation is transferred from one nucleus to another, in this case from the proton to the aluminium. For transfer to take place, the two nuclei must be positioned relatively close. Protons near an aluminium atom intensify the Al signal, whereas in their absence no resonance signal appears in cross-polarisation.

3. Results and discussion

3.1. Slump and mechanical strength

The liquid/KCSA ratio used was 0.5, similar to the value applied in PC, although lower than required for full KCSA hydration (further to water balance Eqs. (1), (2) and (3)). Whereas working with higher ratios might enhance cement hydration, that approach would not be technologically viable because the resulting fresh paste would be overly fluid [28]. In the paste fluidity graph shown in Fig. 2(a) the dashes indicate the cone diameter. As NaOH concentration rose, paste fluidity gradually declined, to 0 for the pastes hydrated with 4 M and 8 M NaOH. Although fluidity was nil in those two samples, the paste was sufficiently plastic and workable to mould the specimens.

The 3 d, 28 d and 90 d compressive strength findings for the reference and experimental pastes are shown in Fig. 2(b). The presence of alkalis had a significant effect on strength development. Whilst the water-hydrated pastes had higher 3 d and 28 d strength than the NaOH-hydrated materials, the 90 d pastes hydrated with 0.1 M and 1 M NaOH exhibited higher strength than the reference, with values of 30.7 MPa and 29.19 MPa, respectively. Higher concentrations induced strength loss. The 90 d specimens bearing 4 M NaOH and the 28 d samples with 8 M NaOH were so severely cracked they could not be tested. Cement cracking and its causes are addressed in the sections below.

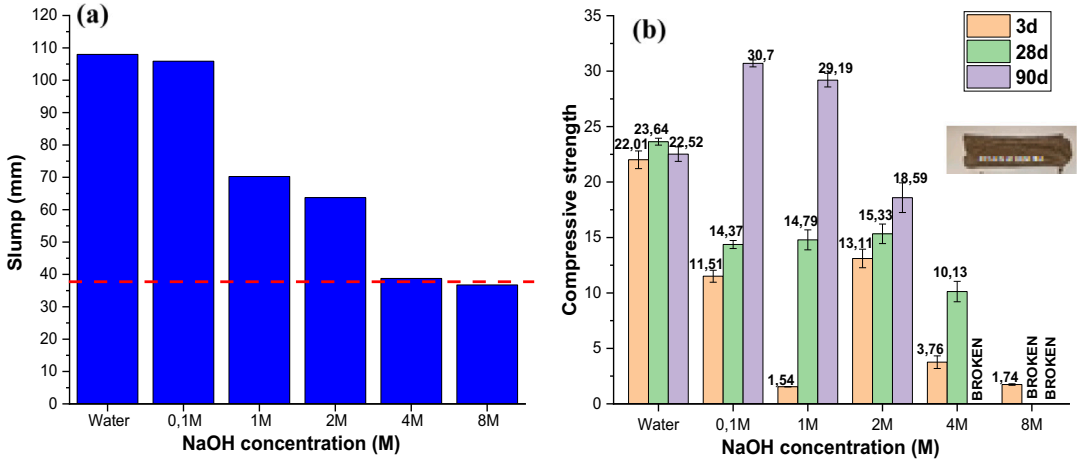

Fig. 2. KCSA pastes hydrated at 0 M, 0.1 M, 1 M, 2 M, 4 M and 8 M NaOH: (a) mini-slump fluidity; (b) 3 d, 28 d and 90 d compressive strength.

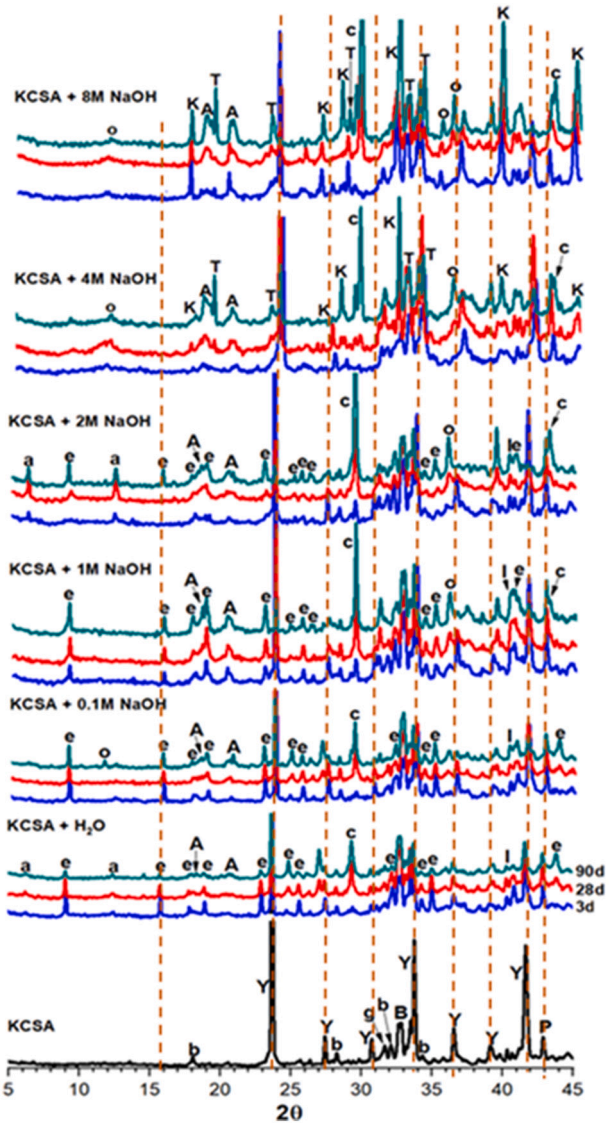

Fig. 3. Diffractograms for anhydrous KCSA and 3 d, 28 d and 90 d water-NaOH-hydrated KCSA pastes.
Legend: Y: ye'elimite ($C_4A_3\bar{S}$, PDF-33-0256); b: belite (C_2S PDF-86-0398); B: bredigite ($Ba_{0.293}Ca_{13.467}Mg_{1.81}Mn_{0.43}O_{32}Si_8$ PDF-36-399); g: gehlenite ($Al_2Ca_2O_7Si$ PDF-35-755); P: periclase (MgO PDF-4-829); e: ettringite ($C_6A\bar{S}_3H_{32}$ PDF-41-1451); A: AH_3 (G: gibbsite (AH_3 PDF-74-1775); I: bayerite (AH_3 PDF-83-2256)); T: thenardite (Na_2SO_4 PDF-37-1465); K: siliceous hydrogarnet = katoite (C_3ASH_4 PDF-84-1354); c: calcite ($CaCO_3$ PDF-86-2334); a: calcium aluminate (CAH_{10} PDF-12-0408CAH_{10}); o: calcium monocarboaluminate (C_4AcH_{11} PDF-87-0493).

3.2. Paste mineralogy: XRD

The XRD patterns for the KCSA clinker and the 3 d, 28 d and 90 d day hydrated pastes are reproduced in Fig. 3. Ye'elimite was the main phase in the starting KCSA, which also contained belite, bredigite, gehlenite, periclase and traces of tricalcium aluminate (C_3A). Ye'elimite diffraction line intensity declined inversely with hydration time, whilst no significant change was observed in the reflections for bredigite, gehlenite or periclase. In the water-hydrated sample, the intensity of the belite diffraction line barely varied, whereas its intensity declined significantly with rising NaOH concentration and longer hydration times. The reflection could not be detected in the materials hydrated with 4 M and 8 M sodium hydroxide, an indication that all the belite had reacted. That finding is consistent with other reports [16], according to which belite hydration was hastened in the presence of alkalis.

Ettringite and aluminium hydroxide (AH_3) were found on the XRD patterns for the reference and the pastes hydrated with 0.1 M, 1 M and 2 M NaOH, in the form of both bayerite and gibbsite, although intensity and resolution (2θ values of 20–21) were low, denoting scant crystallinity or low content [23]. Carbonate in the form of calcite was observed in all the pastes at all three ages, whilst calcium aluminate hydrates (CAH_{10}) were detected in the 28 d and 90 d samples, especially in the pastes hydrated with 2 M NaOH. The intensity of the ettringite line rose with hydration time at concentrations of 0.1 M, 1 M and 2 M, a development associated with the higher degree of reaction in KCSA that would explain the rise in mechanical strength over time (Fig. 2).

Ettringite and CAH_{10} would form as per Eq. (4). Other authors [22,29] observed ettringite to be the main 2 d product of ye'elimite hydration at 20 °C. Winnefeld et al. [8], using GEMS software, found AFm (Eq. (1)) to be thermodynamically favoured over CAH_{10} and ettringite (Eq. (4)) formation and consequently associated the appearance of CAH_{10} with microcrystalline AH_3 solubility. Those authors reported that a 0.3 rise in logarithmic units in the microcrystalline AH_3 solubility product resulted in the reaction described in Eq. (4) rather than in Eqs. (1) or (2). Put another way, the presence of amorphous AH_3 favoured ettringite and CAH_{10} rather than AFm formation. KCSA contains not only ye'elimite, however, but other phases such as C_3A, albeit in small proportions (Table 1) which, along with the water available, affect the type of products formed [24].

The presence of CAH_{10} in pure or 'low sulfate' systems was recently confirmed [24], with pure ye'elimite forming ettringite, CAH_{10} and amorphous aluminium hydroxide (AH_3) rather than the more stable AFm and microcrystalline AH_3. In the 90 d KCSA pastes studied here the ettringite reflection declined slightly whilst the line for AH_3 rose, although no AFm was detected, perhaps due to its low crystallinity. The latter reaction entails volume changes that might largely explain the decline in 28 d and 90 d compressive strength in these pastes (Fig. 2(b)). The foregoing also infers that the presence of CAH_{10} was largely associated with the presence of AH_3 characterised by lower crystallinity than the phase formed as per Eqs. (1) or (2) [8], a particular discussed in greater detail in the section on ^{27}Al MAS NMR.

Ettringite was not detected in the 4 M or 8 M NaOH-hydrated pastes at any of the ages studied. As shown by earlier studies [18,22], ettringite is not stable at very high pH values (pH > 14). AH_3 in the form of gibbsite was detected at all ages, whilst calcium monocarboaluminate (C_4AcH_{11}) formed instead of CAH_{10}. Siliceous hydrogarnet (C_3ASH_4 PDF-84-1354) was also identified, particularly in the 8 M-hydrated pastes, forming as described in the Introduction (Eq. (8)). At the ages tested (3 d, 28 d and 90 d), however, the presence of intermediate phases CH, C-S-H and C_2ASH_8 could not be confirmed, possibly due to the low proportion of belite. As noted earlier, no belite at all was detected in the pastes hydrated with 4 M or 8 M NaOH. Although belite exhibits low reactivity, earlier authors showed that its reaction rate is substantially higher in alkaline media [16,30]. The high alkalinity in these pastes (pH > 14) could vary the equilibrium of those reactions, favouring the formation and precipitation of siliceous hydrogarnet.

Rising alkalinity was also observed to induce thenardite precipitation in the 90 d, 2 M and 4 M NaOH-hydrated pastes and in the 28 d and 90 d 8 M materials. Diffraction line intensity rose with alkalinity and hydration time. Thenardite forms in the presence of excess sodium, which together with the sulfates from ye'elimite dissolution saturate the medium, inducing its precipitation. The presence of this salt was associated with specimen cracking and degradation (Fig. 2(b)), as observed earlier by authors studying CSA cements [26]. Calcite was likewise observed in all the pastes at all ages, with reflection intensity rising with hydration time.

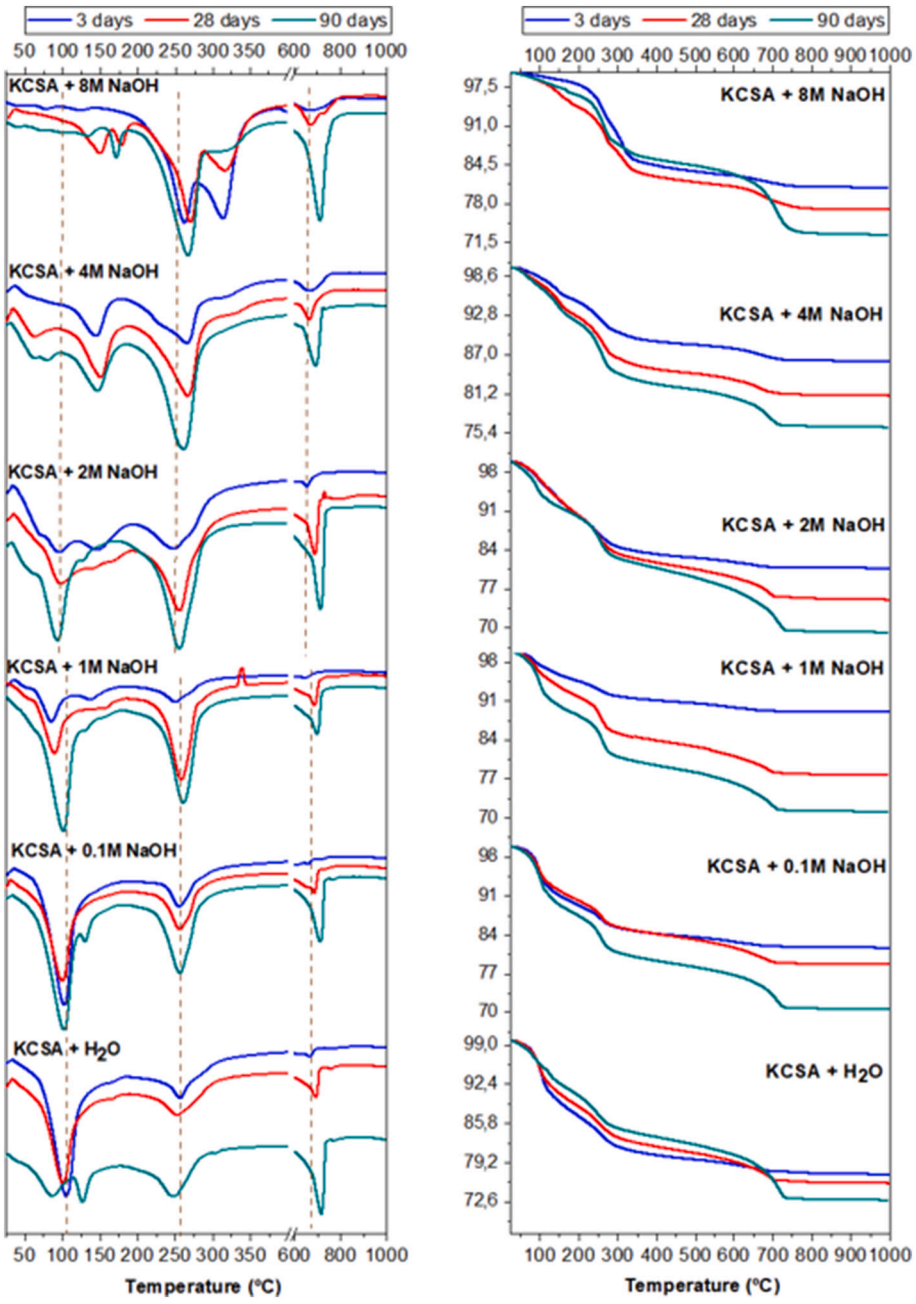

Fig. 4. (a) DTA and (b) TG in water and 0.1 M, 1 M, 2 M, 4 M and 8 M NaOH -hydrated KCSA.

3.3. Differential thermal and thermogravimetric analysis (DTA/TG)

The DTA/TG findings for the 3 d, 28 d and 90 d KCSA pastes hydrated with water and different concentrations of NaOH are shown in Fig. 4. Mass loss up to ≈600 °C is normally related to the water evaporating out of the hydration products formed (AFt, AFm, AH_3, calcium aluminate and carboaluminate hydrates), whereas loss at above that temperature is associated primarily with the release of CO_2 by carbonates such as calcite.

In multi-phase systems the dehydration temperatures of the individual phases often overlap [31]. Ettringite ($3CaO{\cdot}Al_2O_3{\cdot}3CaSO_4{\cdot}32H_2O$) exhibits a hexagonal prismatic structure with columns of octahedral aluminium $[Al(OH)_6]^{3-}$ inter-connected by calcium hydroxide ions $[Ca_6Al_2(OH)_{12}]^{6+}$ and surrounded on the surface by sulfate and water molecules ($[3SO_4{}^{2-}]{\cdot}[26H_2O]^{6-}$). The water molecules evaporate at around 100 °C. AH_3 water loss generates a peak at 210 °C to 280 °C, normally centred over 250/270 °C. Mass loss in CAH_{10} is associated with a peak at 120 °C and in C_3AH_6 at 320 °C, whilst siliceous hydrogarnet (C_3ASH_4) dehydrates at slightly higher temperatures (~340 °C). Calcium monosulfoaluminate ($4CaO{\cdot}Al_2O_3{\cdot}SO_3{\cdot}12H_2O$) may generate up to four peaks that overlap with some of the aforementioned phases: three associated with the loss of its six inter-laminar water molecules (at around 70 °C, 100 °C and most intensely at 170 °C), and the fourth with octahedral layer dehydration, which takes place at higher temperatures (250 °C to 350 °C, most intensely at the latter). Calcium monocarboaluminate ($4CaO{\cdot}Al_2O_3{\cdot}CO_3{\cdot}11H_2O$) exhibits similar behaviour, shedding five water molecules between 60 °C and 200 °C (most intensely at 140 °C) and its six water molecules in the octahedral layer at 200 °C to 300 °C, whilst releasing CO_2 at approximately 650 °C. The position and intensity of these peaks may be affected slightly by inter-phase interaction, the recording conditions and the procedure used to detain hydration [31], all to the

Table 2
Peaks on DTA curves (Fig. 4(a)).

Temperature range	Time (days)	Medium					
		Water	0.1 M	1 M	2 M	4 M	8 M
40–200 °C	3	12.53	10.89	5.35	9.89	5.3	7.23
	28	11.92	10.1	8.32	9.94	7.79	7.54
	90	8.51	12.51	11.69	10.25	8.32	6.27
200–400 °C	3	6.99	4.9	3.62	6.99	5.88	7.58
	28	7.28	5.82	7.73	8.35	7.44	10.08
	90	7.87	8.27	8.99	9.22	9.13	9.66
400–800 °C	3	3.03	2.4	1.9	2.45	2.77	2.7
	28	6.10	5.26	6.14	6.38	3.77	7.27
	90	10.67	8.45	8.11	11.21	12.2	11.3
Total	3	22.50	18.19	10.98	19.31	14.01	17.62
	28	24.55	21.18	22.31	24.94	19.01	25.13
	90	27.05	19.23	28.92	30.84	23.77	27.47

detriment of effective quantification.

The peak at around 100 °C in Fig. 4(a) (signal 1) in the water and 0.1 M, 1 M and 2 M NaOH -hydrated pastes was associated with ettringite decomposition. The endothermal signal at 120/130 °C (signal 2) confirmed the presence of CAH_{10}, although as the signals overlap the weight loss associated with each is difficult to determine. Table 2 lists the weight losses between 40 °C and 200 °C, associated primarily with the two aforementioned phases. Mass loss in that temperature range grew in the pastes hydrated with 0.1 M, 1 M and 2 M dissolutions, whilst it declined in the reference paste. The ettringite reflection on the XRD patterns tended to decline with hydration time in these pastes (KCSA + H_2O). That effect was observed most clearly in the NMR analysis (see Section 3.5). In the DTA curves for the 90 d water-hydrated paste and in the 2 M pastes the ettringite signal shifted to slightly lower temperatures (84 °C). The shift from 100 °C to 85 °C was associated with less crystalline ettringite, although in conjunction with a rise in the intensity of the peak at 120/130 °C it might also be attributable to AFm formation. Whilst that possibility could not be confirmed by XRD, it cannot be ruled out altogether.

Signal 3 at 250/270 °C, associated with AH_3 decomposition, was observed for all the pastes and its intensity grew with hydration time (Tables 2, 200 °C to 400 °C range). The endothermal signal (signal 4) at around 700 °C, generated by carbonate decarbonation, also appeared in all the pastes, likewise with rising intensity over time.

The DTA curve for the 2 M pastes contained an additional peak or shoulder at 140 °C (signal 5), associated with small amounts of C_4AcH_{11} [31]. That signal was much more intense and visible on the 4 M and 8 M hydrated pastes, again growing with hydration time. The curves for those two pastes also exhibited an endothermal or double endothermal signal at 66 °C to 102 °C (signal 6) possibly associated with that phase. The endothermal signal (signal 7) at around 330 °C, in turn, attributed to siliceous hydrogarnet decomposition [31], was most intense in the 3 d, 8 M paste. No signal associated with ettringite decomposition was observed on the DTA curves for the 4 M or 8 M pastes (where XRD detected n ettringite).

3.4. Scanning electron microscopy (SEM)

The 28 d samples hydrated with water, 1 M, 2 M and 8 M NaOH were selected for scanning electron microscopic analysis.

The micrograph of clinker hydrated with distilled water in Fig. 5 shows anhydrous starting phases such as ye'elimite and belite (plates and grains) alongside a mix of hydrate precipitates. Fine ettringite needles are also clearly visible (the EDX analysis revealed the presence of calcium, aluminium and sulfur), along with amorphous and crystalline aluminium hydroxide. The same morphologies can be seen in the 1 M (Fig. 6) and 2 M (Fig. 7) -hydrated pastes, along with CAH_{10} plates or laminae (detail, Fig. 7). AH_3 is either amorphous or forms semi-crystalline laminae or grains. Studies by Chang et al. [23,32] observed mechanical performance to improve when the AH_3 present was more amorphous, for low crystallinity AH_3 filled the voids between the ettringite needles, generating a more compact matrix.

As the micrographs reproduced in Fig. 8 show, the matrix in 8 M NaOH-hydrated KCSA paste differs from that found in other samples. No ettringite needles are present, whilst the hexagonal plates detected are associated with C_4AcH_{11} formation, likewise identified with XRD and DTA. The larger prismatic particles visible in the micrograph denote Na_2SO_4 (thenardite) precipitation.

3.5. Nuclear magnetic resonance

The ^{27}Al MAS NMR spectra for anhydrous clinker and the 3 d and 28 d water-hydrated reference paste and pastes hydrated with 0.1 M, 1 M, 2 M, 4 M and 8 M NaOH are reproduced in Fig. 9, along with the CP MAS NMR for the 28 d pastes.

The wide signal at 67.7 ppm on the spectrum for the anhydrous clinker was attributed to tetrahedral aluminium (Al_T). The spectra for the hydrated pastes show that the intensity of the signals associated with the tetrahedral aluminium in the clinker declined over time, whilst the intensity of the octahedral aluminium (Al_O) signals grew.

Interpreting the ^{27}Al MAS NMR spectrum for the anhydrous KCSA is challenging due to the presence, in addition to ye'elimite, of small proportions of other calcium aluminates (C_3A, gehlenite; Table 1) and quadrupolar interactions. According to the literature, the signals for gehlenite and C_3A both appear at values slightly higher than 74 ppm [21]. In ref. [31] the isotropic chemical shifts for C_3A are reported to be 79.5 ppm and 78.3 ppm (Table 6.3) with reference to the study of Skibsted et al. [33], and at 81 ppm by Andersen et al. [34]. However, the Al_T signals observed here were deemed to be consistent with those reported by other authors for pure synthetic ye'elimite: Sánchez-Herrero et al. [35] at 67.8 ppm and Zhang et al. [23] at 71.4 ppm. To put it another way, the spectrum for KCSA clinker exhibited an Al_T signal practically identical to that observed for synthetic ye'elimite. Further to the ^{27}Al NMR scans, C_3A was either absent or only barely present, i.e., below the ^{27}Al NMR detection limit for Al sites experiencing strong ^{27}Al quandrupole couplings [33]. Those findings are fairly consistent with the Rietveld refinement calculations (Table 1), which revealed a very low C_3A content (~1.75 ± 0.39%).

As a detailed discussion of the Al_T signal generated by ye'elimite lies outside the scope of this article, the reader is referred to a paper published in 2018 by Pedersen et al. [36] on a ^{27}Al magic-angle spinning (MAS) and multiple-quantum (MQ) MAS NMR study of ye'elimite, using six magnetic fields from 4.7 T to 22.3 T. By way of summary and of indication of the complexity of that study, the authors differentiated eight positions for AlO_4, four of which doubled the intensity shared by the other four. The positions defined were based on the Pcc2 orthorhombic structural model proposed by Calos et al. [37] for ye'elimite, later refined by Cuesta et al. [38]. Although with certain minor differences, both groups of authors proposed a structure using the same indexing of aluminium atoms, where Al (1) to Al (4) exhibited multiplicities of 2 and Al (5) to Al (8) multiplicities of 4. The eight sites occupied similar chemical positions on the ^{27}Al spectrum, but exhibited different quadrupole coupling, with signals ranging from +76 ppm to +73 ppm in KCSA spectrum, for the 9.4 T magnetic field used here. (Field strength has also been found to affect the results [36]).

The primary focus of the present study was an analysis of the Al_O signal and the determination of ΣAl_O to roughly establish the degree of reaction of ye'elimite, the majority phase in KCSA. In the water- and 0.1 M-hydrated KCSA pastes, the signal for Al_O had two peaks, one centred at 13.2 ppm and the other at 9.5 ppm. The intensity of the former declined whilst the latter grew more intense with rising alkalinity. Many authors have identified aluminate hydrate phases on the grounds of their position on ^{27}Al MAS NMR spectra. According to most, ettringite generates a signal at 13.2 ppm [31,34,35,39,40]; katoite

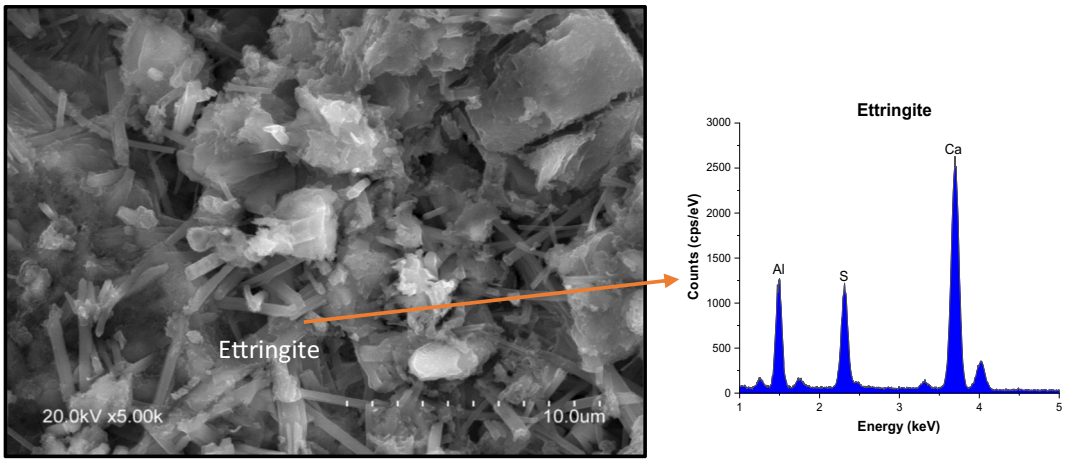

Fig. 5. SEM micrograph of 28 days, water-hydrated clinker.

(C_3AH_6) at 12.4 ppm [31,35,39,40]; AFm at 11.6 ppm [31]; CAH_{10} at 9.5 ppm [39]; and C_4AcH_{11} also at 9.5 ppm [31,35,40]. The values given for AH_3 vary, however. Gastaldi et al. [21] observed the signal at 11.8 ppm, whereas Skibsted et al. [39] reported finding two non-equivalent Al atoms in octahedral environments at 10.4 ± 0.3 ppm (Al (l)) and 11.5 ± 0.3 ppm (Al(2)) in synthetic γ-AH_3 applying a magnetic field strength of 9.4 T. (This signal appears at lower chemical shifts (< 8 ppm) in amorphous alumina gel.) Zhang and Chang [23], in turn, observed the signal at 9.3 ppm and Isobe et al. [41] at 7.5 ppm. The differences in AH_3 position may be associated, generally speaking, with the greater or lesser crystallinity of the hydroxide: higher crystallinity generates higher ppm values and vice-versa. Andersen et al. [42] identified another octahedral aluminium at values under 5 ppm in hydrated PC pastes, which they called the third aluminate hydrate (TAH). They [42] contended that TAH comprises calcium aluminate hydrate or aluminate hydrate phases and/or precipitates lying on C-S-H particle surfaces. Those aluminium phases were not detected by XRD, in all likelihood due to their low crystallinity or small crystal size, but at the same time they cannot not be overlooked, for large quantities of octahedral aluminium are trapped in their structure. As discussed below, the deconvolution of the ^{27}Al spectra for some of the hydrated pastes studied here suggested the possible presence of such aluminium: [12] crystalline, microcrystalline and amorphous.

KCSA hydration is complex and the precipitates are particularly difficult to identify and quantify because their signals overlap on the spectrum. The ^{27}Al MAS NMR spectra were consequently deconvoluted to better interpret the results. Deconvolution was based on both ^{1}H−^{27}Al CP/MAS NMR findings and an analysis of the second derivative to determine the number and position of the signals.

None of the CP/MAS NMR (technique in which the proximity of protons or OH groups enhances the signal of Al atoms) [11,12] spectra in Fig. 9 contains an Al_T signal, confirming the absence of this species in all the hydrated phases, which consequently comprise Al_O. When ^{1}H−^{27}Al cross-polarisation (CP) MAS NMR was conducted on the water, 0.1 M and 1 M NaOH -hydrated pastes, the intensity of the signal at 13.2 ppm was substantially enhanced, clearly denoting the presence of ettringite. In contrast, the signal disappeared in the CP/MAS NMR spectra for the pastes hydrated with 4 M and 8 M sodium hydroxide. That development was consistent with non-detection of the mineral in XRD and DTA/TG analysis due to its instability-determined failure to form at that alkalinity.

In light of the foregoing, analysis of the second derivative to determine the number and position of the hydrated phases was conducted only for the Al_O signal. This mathematical method, here applied with Origin9 software, identifies the presence of the relative maxima and minima of a mathematical function. The example in Fig. 10 shows the maxima found for some of the spectra. Phase crystallinity was associated with band width, i.e., narrower signals were deemed to denote crystalline phases and a more orderly local environment.

Fig. 11 illustrates the results of the deconvolution, performed on the grounds of the above two criteria using dmfit software and assuming the signals to have a Gaussian/Lorentzian (0.5) profile.

The signal for anhydrous KCSA, also included in the deconvolution (Fig. 11; more detailed information in supplementary Table 3) to

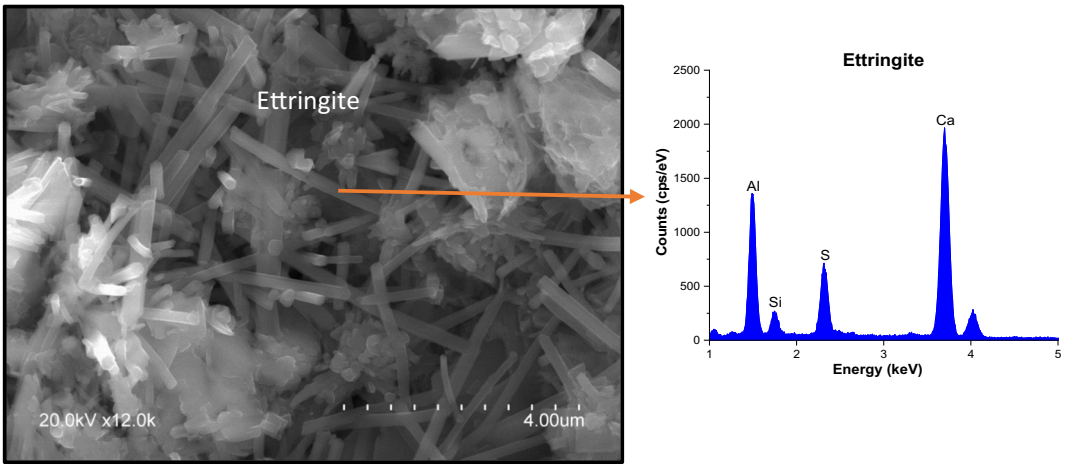

Fig. 6. SEM micrograph of 28 days, 1 M NaOH-hydrated clinker.

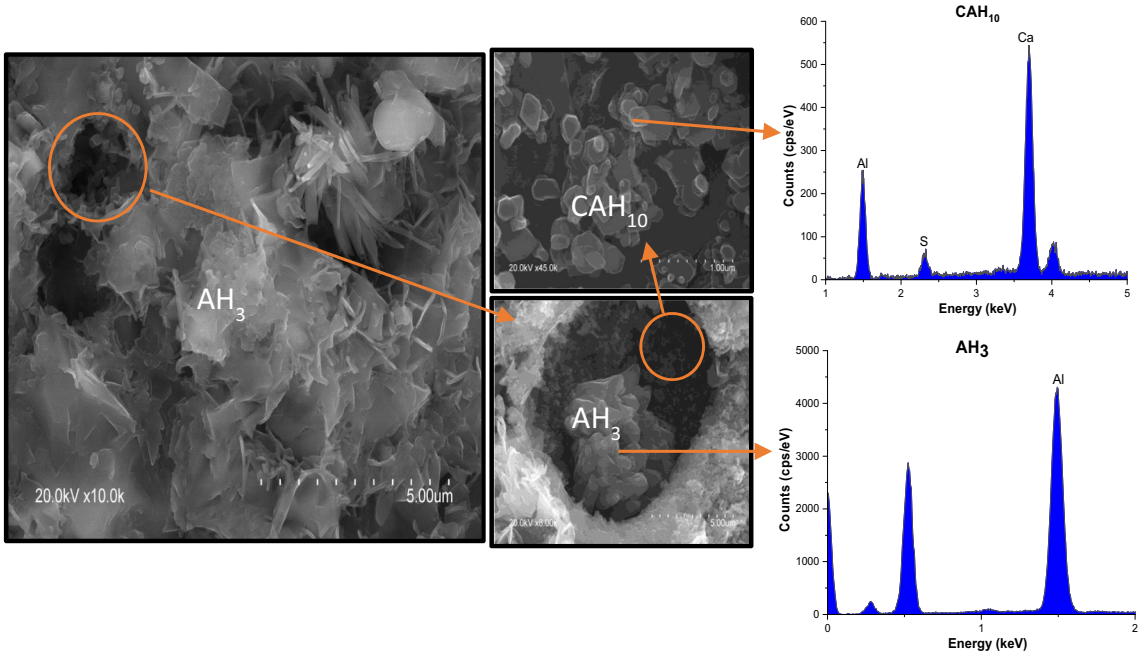

Fig. 7. SEM micrograph of 28 days, 2 M NaOH-hydrated clinker.

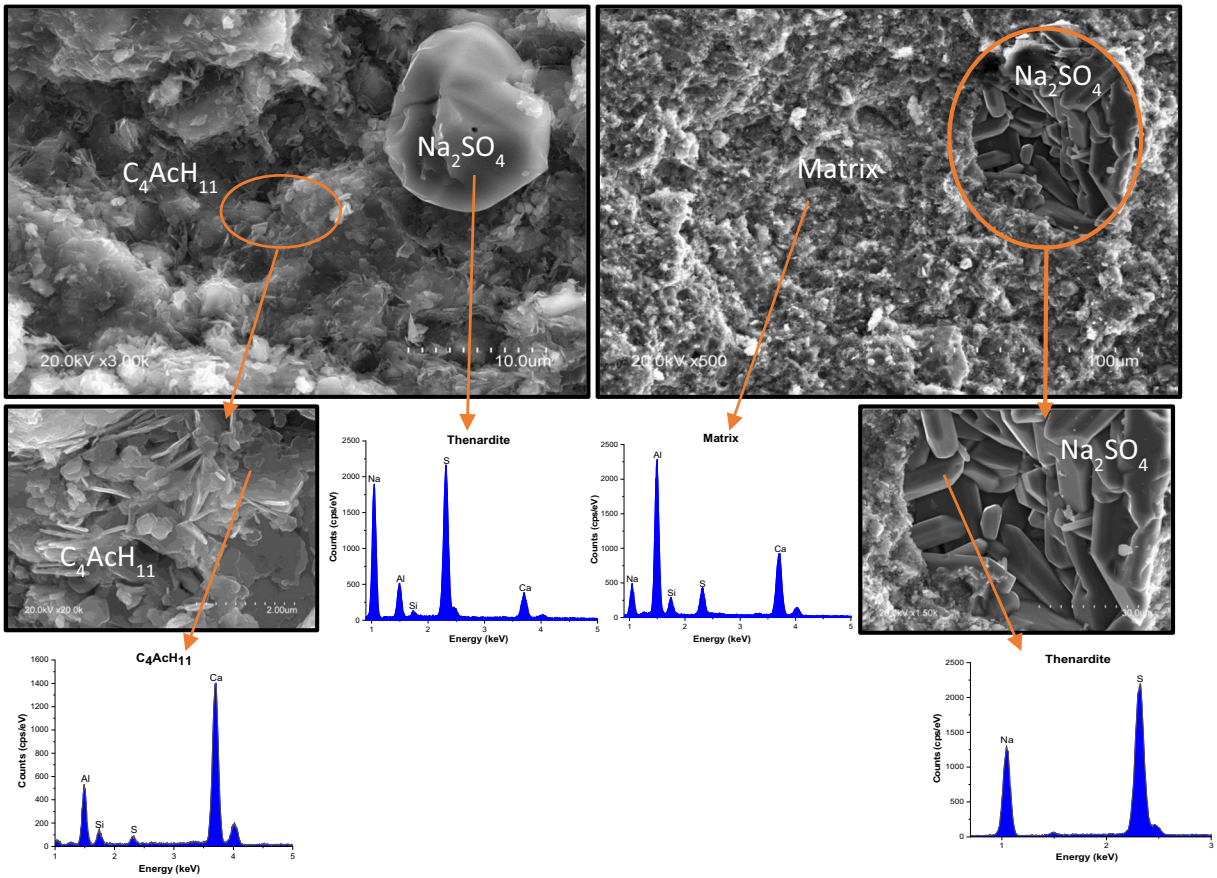

Fig. 8. SEM micrograph of 28 days, 8 M NaOH-hydrated clinker.

occupy area, three signals were used at 60 ppm, 62 ppm and 52 ppm. Due to signal complexity as a result of the inclusion of quadrupolar interactions, it was used only as an option for determining the amount of unreacted Al_T. The Al_O signal on the hydrated paste spectra was deconvoluted into three bands, further to the information delivered by the second derivative. In most of the spectra, a fourth band at values of under 5 ppm also had to be included, however. The authors considers that it is associated with the presence of a SEM-detected, gel-like amorphous aluminium hydroxide. As noted earlier, this phase, a species known as TAH [42], was also identified on ^{27}Al spectra for other

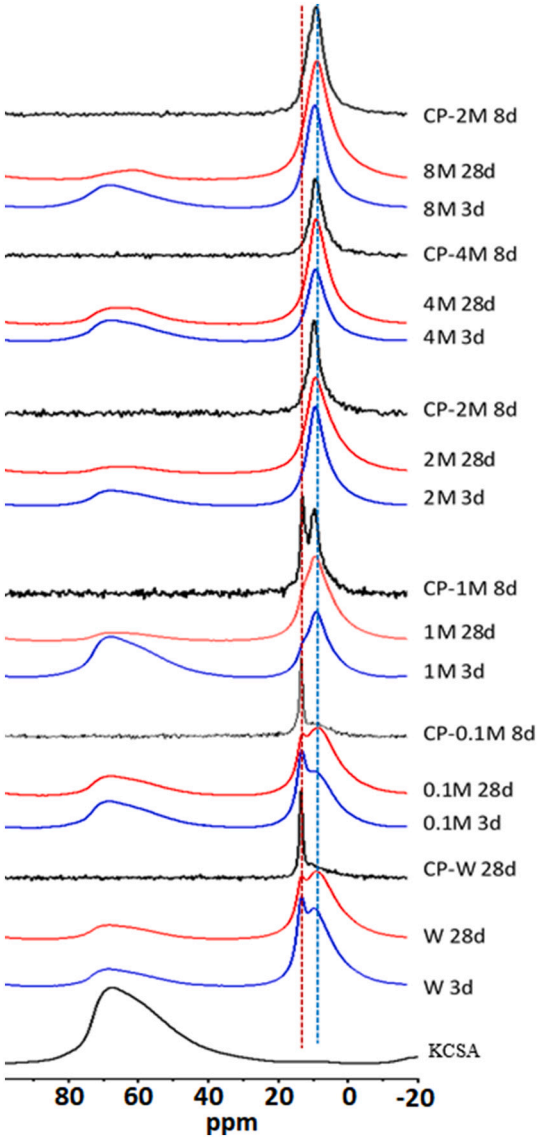

Fig. 9. ^{27}Al MAS NMR spectra for anhydrous KCSA and 3 d and 28 d hydrated pastes.

cementitious materials.

The results in Fig. 11 show that the 3 d water and 0.1 M -hydrated pastes generated a predominant signal (recorded in the octahedral aluminium region at 13.3 ppm) attributed to ettringite. Another signal with similar intensity at 9.5 ppm was associated with calcium aluminate hydrates such as the CAH_{10} and C_4AcH_{11} detected by XRD. An overlapping band associated with a gibbsite-like crystalline AH_3 was also present in this region. The intensity of the ettringite signal declined in the 28 d materials, whilst the signal at +9.5 ppm grew.

The band at values of around 8/7 ppm was attributed to an aluminium hydroxide with lower, i.e., nano-crystallinity. Using ptychographic X-ray computed tomography, Cuesta et al. [43] showed that the AH_3 present in CSA cements has a nano-gibbsite local structure with a particle size of 3 nm to 4 nm. They nonetheless observed that the aforementioned structure may be impacted by the uptake of small proportions of Ca ions governed by the amount of water, presence of sulfate or pH. Lastly, a signal was obtained for values of under 4 ppm, associated with a gel-like disorderly aluminium hydroxide or TAH. The generation of different signals by AH_3 is related to its various degrees of crystallinity.

The ettringite signal on the spectrum for the 3 d, 2 M NaOH-hydrated KCSA was less intense. The signal at 9.5 ppm on both the 3 d and 28 d spectra was associated with calcium aluminates (CAH_{10} and C_4AcH_{11}) and a gibbsite-like crystalline AH_3; the signal at 8/7 ppm was again attributed to amorphous or nano-crystalline AH_3. The signal for the aluminium hydroxide gel or TAH appeared at values of under 4 ppm.

Whilst no ettringite was detected in the 4 M or 8 M NaOH pastes, three signals were observed: at 12.6 ppm, associated with hydrogarnet, at 9.5 ppm with calcium carboaluminate and at 6.0 ppm with aluminium hydroxide. A further signal had to be included at 2 ppm on the 28 d, 8 M spectrum, attributed to an aluminium gel.

The graph in Fig. 12 compares the areas associated with the Al_O signals generated by the mineral phases: the taller the bar, the higher the degree of reaction of the aluminium-high phase, in this case ye'elimite. The 3 d and 28 d values for the water-hydrated material were fairly similar and greater than 80%, findings consistent with strength development as shown in Fig. 2(b). Greater differences in intensity were observed between the 3 d and 28 d pastes hydrated with 0.1 M, 1 M or 2 M NaOH solutions, although the reaction products were the same. Those data denote a certain delay in the hydration reactions that would explain the low early age and high later age strength observed in these mixes. The degree of reaction in the 3 d 4 M and 8 M materials was lower than in the reference, but rose after 28 d. Here, however, the hydration products differed, for thenardite was detected and ettringite absent. These findings are consistent with the results reported by Zhang et al. [23,32].

The data graphed in Fig. 12 confirmed the absence of ettringite in the 4 M- and 8 M-hydrated pastes observed in XRD and DTA. The signal at 9.5 ppm was associated with the overlap of calcium aluminate hydrates and carboaluminates and possibly gibbsite-like crystalline AH_3. The intensity of that signal grew substantially with solution alkalinity, denoting a higher degree of crystallinity in those phases.

The area of the signal at 8/7 ppm, attributed to an amorphous-nano-crystalline AH_3 weakly detected by XRD rose with alkali concentration. In contrast, the intensity of the signal at values lower than 4 ppm

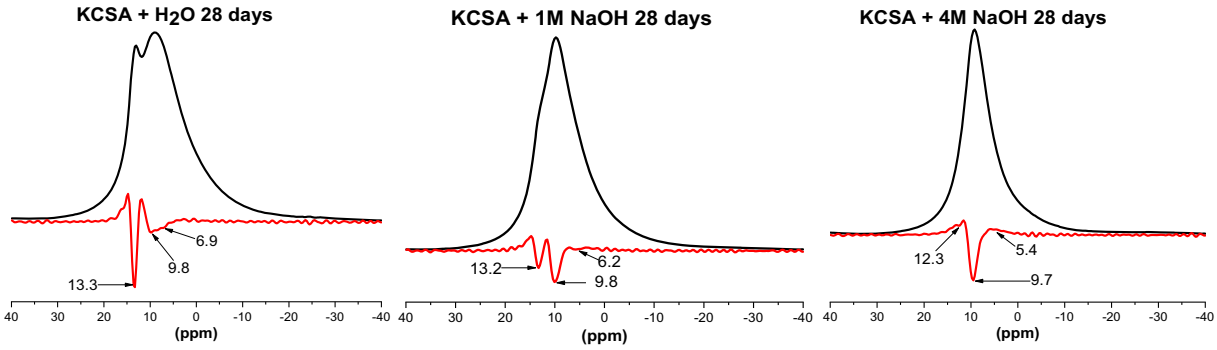

Fig. 10. Analysis of the second derivative for ^{27}Al MAS NMR spectra generated by 3 d, 1 M and 4 M NaOH-hydrated KCSA paste.

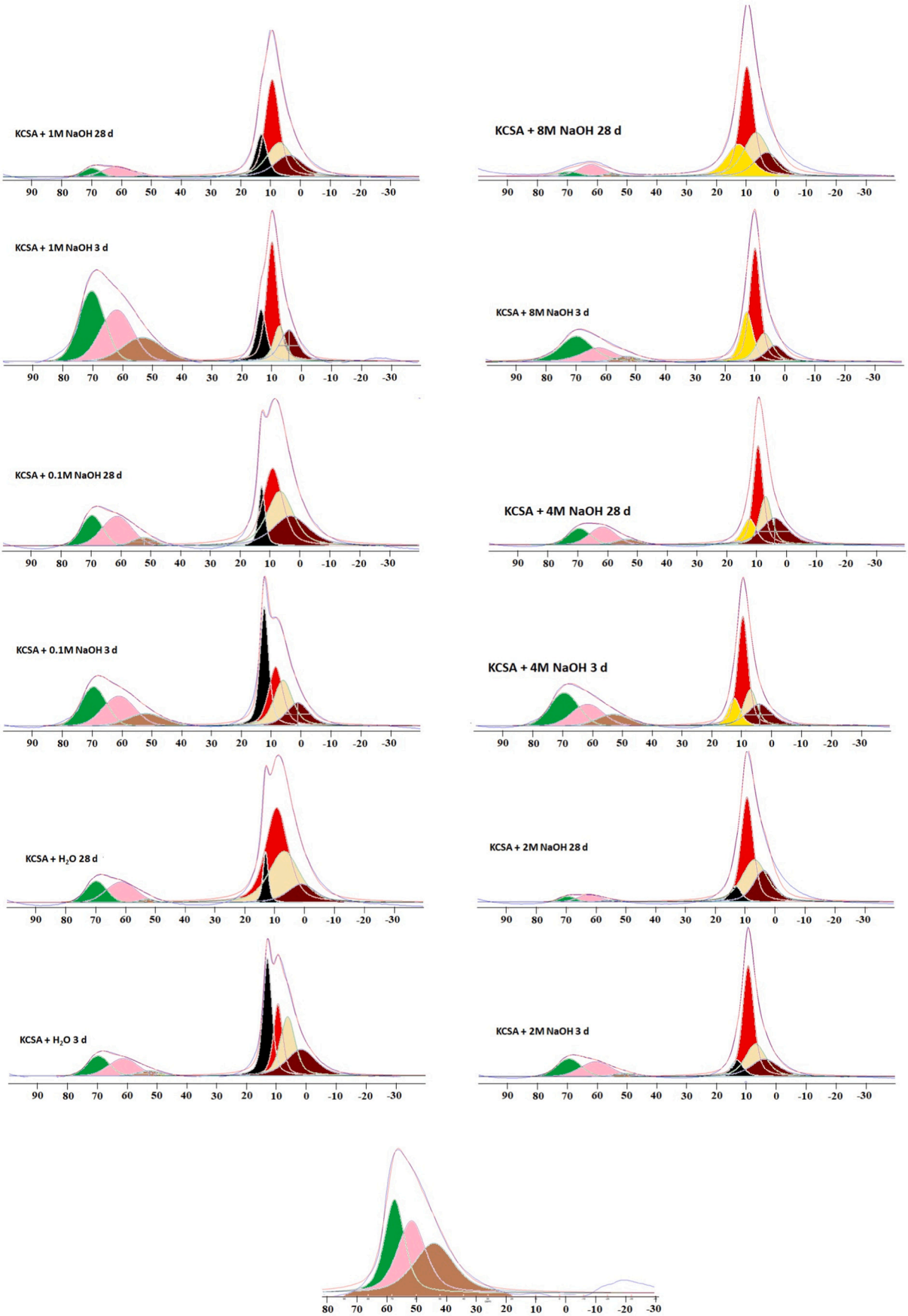

Fig. 11. NMR deconvolution: 13.3 = black; 12.40 = yellow; 9.5 = red; 8/7 = light grey; < 4 = maroon. (For interpretation of the references to colour in this figure legend, the reader is referred to the web version of this article.)

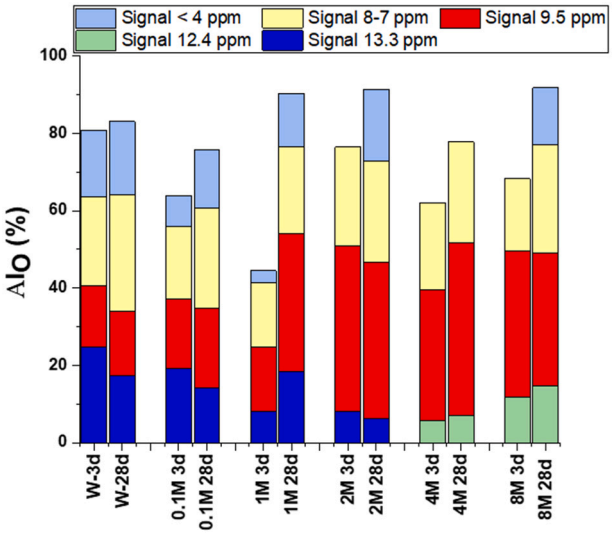

Fig. 12. Relative areas associated with Al_O signals in ^{27}Al MAS NMR spectra.

decreased with rising concentration and at 4 M was undetected. These findings corroborate the observation that alkaline concentrations also affects AH_3 microstructure.

KCSA hydrated rapidly, given that the l/s ratio used was 0.5, under which conditions AH_3 or ettringite crystals are afforded scant space or time to grow. The SEM micrographs clearly revealed the presence of ettringite crystals, whereas the AH_3 exhibited low crystallinity, with the respective crystals only readily visible when developing in pores/cavities in the matrix (Fig. 7). The rate of reaction was retarded at higher pH levels, which may have allowed more time for larger crystals to grow.

The proportion of AH_3 (signals at 9.5 ppm and < 4 ppm) in the 4 M and 8 M pastes (~20% to 25%) was significantly lower than the percentage in the pastes hydrated with water, 0.1 M, 1 M and 2 M NaOH (~40%) for fairly similar degrees of reaction. The inference is that the AH_3 in the 4 M and 8 M pastes may have reacted with the silica in C_2S to form hydrogarnet. Equilibrium was modified in Eqs. (5) and (6) due to the high pH in the medium, favouring hydrogarnet precipitation, even though the intermediate phases were not detected at the ages studied. Thermodynamic studies would be advisable to explore that premise.

In the DTA and XRD analyses of paste 8 M the intensity of the hydrogarnet signal declined over time. NMR revealed the presence of amorphous AH_3 in the 28 d paste (signal at < 4 ppm), absent in the 3 d material. That gel-like amorphous AH_3 may have been formed during secondary hydrogarnet carbonation in a process similar to that described in Eq. (8). Katoite is highly susceptible to carbonation, a development favoured by high pH and associated with major changes in volume which, together with the presence of thenardite, induces paste cracking. Similar behaviour was observed in pure ye'elimite hydration with 8 M NaOH [22].

$$3CaO{\cdot}Al_2O_3{\cdot}6H_2O + 3CO_2 \rightarrow 3CaCO_3 + 2Al(OH)_3\,(gel) + 3H_2O \quad (8)$$

4. Conclusions

This study aimed to explore the effect of different alkali contents on KCSA hydration with a view to using that clinker in blended or hybrid alkaline cements. The cements were hydrated at w/c = 0.5, a value lower than required for all the KCSA to hydrate but sufficient to ensure good paste workability. The 3 d, 28 d and 90 d findings showed that a low alkaline content (0.1 M or 1 M) has a beneficial effect on later age binders. In contrast, high alkalinity impacts strength development adversely, more significantly over time.

The presence of alkalis at low or moderate concentrations (0.1 M, 1 M or 2 M) retards KCSA hydration slightly, although the hydration products formed are similar to those observed with water hydration (ettringite, CAH_{10} and AH_3). That slower reaction rate explains the lower early age mechanical strength found for these materials, and the subsequent rise in strength at later ages in response to the higher degree of KCSA reaction, as well as to the presence of crystalline hydrates.

As at high alkalinities (4 M and 8 M) ettringite is unstable it fails to form, whereas thenardite precipitates. The AH_3 formed under such conditions exhibits higher crystallinity and may react with C_2S to form siliceous hydrogarnet. That likewise unstable phase may carbonate, forming calcite and an aluminium gel that would induce cracking and a decline in later age mechanical strength.

Declaration of competing interest

The authors declare that they have no known competing financial interests or personal relationships that could have appeared to influence the work reported in this paper.

Acknowledgements

This research was developed thanks to the support of the Ministry of Science and Innovation and Universities and FEDER funds that subsidize the Project BIA2016-76466-R and the aid BES-2017-082022. In addition, the PhD student Pilar Padilla-Encinas, thanks to the University Autónoma of Madrid, to be able to carry out her thesis in the Applied Chemistry program. Also thanks to HeidelbergCement Hispania for supplying the clinker.

Appendix A. Supplementary data

Supplementary data to this article can be found online at https://doi.org/10.1016/j.cemconres.2020.106251.

References

[1] I.A. Chen, M.C.G. Juenger, Incorporation of coal combustion residuals into calcium sulfoaluminate-belite cement clinkers, Cem. Concr. Compos. 34 (2012) 893–902, https://doi.org/10.1016/j.cemconcomp.2012.04.006.
[2] F.P. Glasser, L. Zhang, High-performance cement matrices based on calcium sulfoaluminate–belite compositions, Cem. Concr. Res. 31 (2001) 1881–1886, https://doi.org/10.1016/S0008-8846(01)00649-4.
[3] Borje Ost, Benedict Schiefelbein, John Summerfield, Very high early strength cement, US Patent No. 3860433 (1975).
[4] P. Chaunsali, P. Mondal, Influence of calcium sulfoaluminate (CSA) cement content on expansion and hydration behavior of various ordinary portland cement-CSA blends, J. Am. Ceram. Soc. 98 (2015) 2617–2624, https://doi.org/10.1111/jace.13645.
[5] G. Le Saoût, B. Lothenbach, A. Hori, T. Higuchi, F. Winnefeld, Hydration of Portland cement with additions of calcium sulfoaluminates, Cem. Concr. Res. 43 (2013) 81–94, https://doi.org/10.1016/j.cemconres.2012.10.011.
[6] F. Winnefeld, B. Lothenbach, Hydration of calcium sulfoaluminate cements — experimental findings and thermodynamic modelling, Cem. Concr. Res. 40 (2010) 1239–1247, https://doi.org/10.1016/j.cemconres.2009.08.014.
[7] S. Kramar, L. Žibret, E. Fidanchevska, V. Jovanov, B. Angjusheva, V. Ducman, Use of fly ash and phosphogypsum for the synthesis of belite-sulfoaluminate clinker, Mater. Constr. 69 (2019) 176, https://doi.org/10.3989/mc.2019.11617.
[8] F. Winnefeld, B. Lothenbach, Phase equilibria in the system $Ca_4Al_6O_{12}SO_4$ – Ca_2SiO_4 – $CaSO_4$ – H_2O referring to the hydration of calcium sulfoaluminate cements, RILEM Tech. Lett. 7 (2016).
[9] T. Matschei, B. Lothenbach, F.P. Glasser, The AFm phase in Portland cement, Cem. Concr. Res. 37 (2007) 118–130, https://doi.org/10.1016/j.cemconres.2006.10.010.
[10] J. Wang, I. Baco, V. Morin, G. Walenta, D. Damidot and E. Gartne, Hydration mechanism of cements based on low-CO_2 clinkers containing belite, ye'elimite and calcium alumino-ferrite, Conference: The 7th International Symposium on Cement & Concrete ISCC2010. At Jinan, China, Volume: Session 1.
[11] F. Song, Z. Yu, F. Yang, Y. Lu, Y. Liu, Microstructure of amorphous aluminum hydroxide in belite-calcium sulfoaluminate cement, Cem. Concr. Res. 71 (2015) 1–6, https://doi.org/10.1016/j.cemconres.2015.01.013.
[12] D. Jansen, J.J. Wolf, N. Fobbe, The hydration of nearly pure ye'elimite with a sulfate carrier in a stoichiometric ettringite binder system. Implications for the hydration process based on in-situ XRD, ^{1}H-TD-NMR, pore solution analysis, and

thermodynamic modeling, Cem. Concr. Res. 127 (2020) 105923, , https://doi.org/10.1016/j.cemconres.2019.105923.
[13] F. Winnefeld, S. Barlag, Calorimetric and thermogravimetric study on the influence of calcium sulfate on the hydration of ye'elimite, J. Therm. Anal. Calorim. 101 (2010) 949–957, https://doi.org/10.1007/s10973-009-0582-6.
[14] V. Kasselouri, P. Tsakiridis, Ch. Malami, B. Georgali, C. Alexandridou, A study on the hydration products of a non-expansive sulfoaluminate cement, Cem. Concr. Res. 25 (1995) 1726–1736, https://doi.org/10.1016/0008-8846(95)00168-9.
[15] I.A. Chen, C.W. Hargis, M.C.G. Juenger, Understanding expansion in calcium sulfoaluminate–belite cements, Cem. Concr. Res. 42 (2012) 51–60, https://doi.org/10.1016/j.cemconres.2011.07.010.
[16] M.J. Sánchez-Herrero, A. Fernández-Jiménez, Á. Palomo, Alkaline hydration of C_2S and C_3S, J. Am. Ceram. Soc. 99 (2016) 604–611, https://doi.org/10.1111/jace.13985.
[17] M.C.G. Juenger, F. Winnefeld, J.L. Provis, J.H. Ideker, Advances in alternative cementitious binders, Cem. Concr. Res. 41 (2011) 1232–1243, https://doi.org/10.1016/j.cemconres.2010.11.012.
[18] M. Ben Haha, F. Winnefeld, A. Pisch, Advances in understanding ye'elimite-rich cements, Cem. Concr. Res. 123 (2019) 105778, , https://doi.org/10.1016/j.cemconres.2019.105778.
[19] R.J. Myers, E. L'Hôpital, J.L. Provis, B. Lothenbach, Effect of temperature and aluminium on calcium (alumino)silicate hydrate chemistry under equilibrium conditions, Cem. Concr. Res. 68 (2015) 83–93, https://doi.org/10.1016/j.cemconres.2014.10.015.
[20] J. Haas, A. Nonat, From C–S–H to C–A–S–H: experimental study and thermodynamic modelling, Cem. Concr. Res. 68 (2015) 124–138, https://doi.org/10.1016/j.cemconres.2014.10.020.
[21] D. Gastaldi, G. Paul, L. Marchese, S. Irico, E. Boccaleri, S. Mutke, L. Buzzi, F. Canonico, Hydration products in sulfoaluminate cements: evaluation of amorphous phases by XRD/solid-state NMR, Cem. Concr. Res. 90 (2016) 162–173, https://doi.org/10.1016/j.cemconres.2016.05.014.
[22] M.J. Sánchez-Herrero, A. Fernández-Jiménez, A. Palomo, $C_4A_3\check{S}$ hydration in different alkaline media, Cem. Concr. Res. 46 (2013) 41–49, https://doi.org/10.1016/j.cemconres.2013.01.008.
[23] Y. Zhang, J. Chang, Microstructural evolution of aluminum hydroxide gel during the hydration of calcium sulfoaluminate under different alkali concentrations, Constr. Build. Mater. 180 (2018) 655–664, https://doi.org/10.1016/j.conbuildmat.2018.06.010.
[24] F. Bullerjahn, E. Boehm-Courjault, M. Zajac, M. Ben Haha, K. Scrivener, Hydration reactions and stages of clinker composed mainly of stoichiometric ye'elimite, Cem. Concr. Res. 116 (2019) 120–133, https://doi.org/10.1016/j.cemconres.2018.10.023.
[25] K. Ogawa, D.M. Roy, $C_4A_3\bar{S}$ hydration, ettringite formation, and its expansion mechanism III. Effect of CaO, NaOH and NaCl. Conclusions, Cem. Concr. Res. 12 (1982) 247–256.
[26] L.U.D. Tambara, M. Cheriaf, J.C. Rocha, A. Palomo, A. Fernández-Jiménez, Effect of alkalis content on calcium sulfoaluminate (CSA) cement hydration, Cem. Concr. Res. 128 (2020) 105953, , https://doi.org/10.1016/j.cemconres.2019.105953.
[27] A. Palomo, P. Krivenko, I. Garcia-Lodeiro, E. Kavalerova, O. Maltseva, A. Fernández-Jiménez, A review on alkaline activation: new analytical perspectives, Mater. Constr. 64 (2014) e022, https://doi.org/10.3989/mc.2014.00314.
[28] L. Zhang, F.P. Glasser, Hydration of calcium sulfoaluminate cement at less than 24 h, Adv. Cem. Res. (2002) 15.
[29] W. Lan, F.P. Glasser, Hydration of calcium sulphoaluminate cements, Adv. Cem. Res. 8 (1996) 127–134, https://doi.org/10.1680/adcr.1996.8.31.127.
[30] M.J. Sánchez-Herrero, A. Fernández-Jiménez, A. Palomo, C_3S and C_2S hydration in the presence of Na_2CO_3 and Na_2SO_4, J. Am. Ceram. Soc. 100 (2017) 3188–3198, https://doi.org/10.1111/jace.14855.
[31] K. Scrivener, R. Snellings, B. Lothenbach, A Practical Guide to Microstructural Analysis of Cementitious Materials, 0 ed., CRC Press, 2018, https://doi.org/10.1201/b19074.
[32] Y. Zhang, J. Chang, J. Ji, AH_3 phase in the hydration product system of AFt-AFm-AH_3 in calcium sulfoaluminate cements: a microstructural study, Constr. Build. Mater. 167 (2018) 587–596, https://doi.org/10.1016/j.conbuildmat.2018.02.052.
[33] J. Skibsted, H. Bildse, H.J. Jakobsen, High-speed spinning versus high magnetic field in MAS NMR of quadrupolar nuclei. ^{27}A1 MAS NMR of 3CaO. $A1_2O_3$, J. of Magnetic Resonance 92 (1991) 669–676.
[34] M.D. Andersen, H.J. Jakobsen, J. Skibsted, Incorporation of aluminum in the calcium silicate hydrate (C − S − H) of hydrated portland cements: a high-field ^{27}Al and ^{29}Si MAS NMR investigation, Inorg. Chem. 42 (2003) 2280–2287, https://doi.org/10.1021/ic020607b.
[35] M.J.S. Herrero, La Activación Alcalina como Procedimiento para el Desarrollo de Nuevos Cementos Belíticos, (2017), p. 376.
[36] M.T. Pedersen, F. Jensen, J. Skibsted, Structural investigation of ye'elimite, $Ca_4Al_6O_{12}SO_4$, by ^{27}Al MAS and MQMAS NMR at different magnetic fields, J. Phys. Chem. C 122 (2018) 12077–12089, https://doi.org/10.1021/acs.jpcc.8b02497.
[37] N.J. Calos, C.H.L. Kennard, A.K. Whittaker, R.L. Davis, Structure of calcium aluminate sulfate $Ca_4Al_6O_{16}S$, J. Solid State Chem. 119 (1995) 1–7.
[38] A. Cuesta, A.G. De la Torre, E.R. Losilla, V.K. Peterson, P. Rejmak, A. Ayuela, C. Frontera, M.A.G. Aranda, Structure, atomistic simulations, and phase transition of stoichiometric yeelimite, Chem. Mater. 25 (2013) 1680–1687, https://doi.org/10.1021/cm400129z.
[39] J. Skibsted, E. Henderson, H.J. Jakobsen, Characterization of calcium aluminate phases in cements by aluminum-^{27}Al MAS NMR spectroscopy, Inorg. Chem. 32 (1993) 1013–1027, https://doi.org/10.1021/ic00058a043.
[40] P. Faucon, T. Charpentier, D. Bertrandie, A. Nonat, J. Virlet, J.C. Petit, Characterization of calcium aluminate hydrates and related hydrates of cement pastes by ^{27}Al MQ-MAS NMR, Inorg. Chem. 37 (1998) 3726–3733, https://doi.org/10.1021/ic9800076.
[41] T. Isobe, T. Watanabe, J.B. d'Espinose de la Caillerie, A.P. Legrand, D. Massiot, Solid-state ^{1}H and ^{27}Al NMR studies of amorphous aluminum hydroxides, J. Colloid Interface Sci. 261 (2003) 320–324, https://doi.org/10.1016/S0021-9797(03)00144-9.
[42] M.D. Andersen, H.J. Jakobsen, J. Skibsted, A new aluminium-hydrate species in hydrated Portland cements characterized by ^{27}Al and ^{29}Si MAS NMR spectroscopy, Cem. Concr. Res. 36 (2006) 3–17, https://doi.org/10.1016/j.cemconres.2005.04.010.
[43] A. Cuesta, A.G. De la Torre, I. Santacruz, P. Trtik, J.C. da Silva, A. Diaz, M. Holler, M.A.G. Aranda, Chemistry and mass density of aluminum hydroxide gel in eco-cements by ptychographic X-ray computed tomography, J. Phys. Chem. C 121 (2017) 3044–3054, https://doi.org/10.1021/acs.jpcc.6b10048.